analytical chemistry

Article

pubs.acs.org/ac

Raman Spectroscopy Enables Noninvasive Biochemical Characterization and Identification of the Stage of Healing of a Wound

Rishabh Jain,[†] Diego Calderon,[‡] Patricia R. Kierski,[‡] Michael J. Schurr,[§] Charles J. Czuprynski,[∥] Christopher J. Murphy,[⊥,¶] Jonathan F. McAnulty,*[,‡] and Nicholas L. Abbott*[,†]

[†]Department of Chemical and Biological Engineering, University of Wisconsin-Madison, Madison, Wisconsin 53706, United States

[‡]Department of Surgical Sciences, School of Veterinary Medicine, University of Wisconsin-Madison, Madison, Wisconsin 53706, United States

[§]Department of Surgery, School of Medicine and Public Health, University of Colorado-Denver, Denver, Colorado 80217 United States

[∥]Department of Pathobiological Sciences, School of Veterinary Medicine, University of Wisconsin-Madison, Madison, Wisconsin 53706, United States

[⊥]Department of Surgical and Radiological Sciences, School of Veterinary Medicine, University of California-Davis, Davis, California 95616, United States

[¶]Department of Ophthalmology & Vision Science, School of Medicine, University of California-Davis, Davis, California 95616, United States

Supporting Information

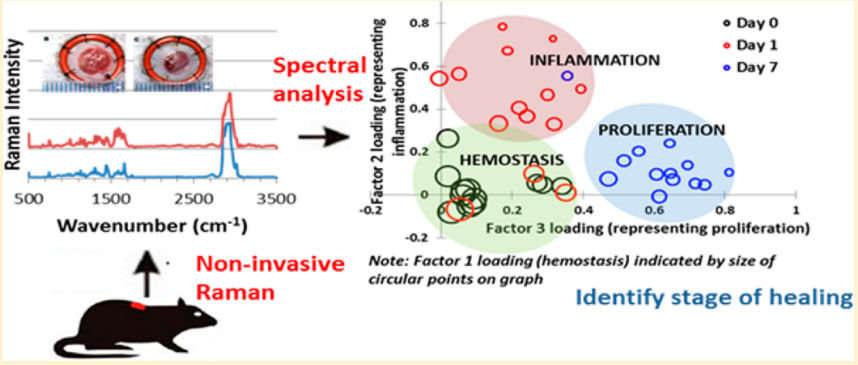

ABSTRACT: Accurate and rapid assessment of the healing status of a wound in a simple and noninvasive manner would enable clinicians to diagnose wounds in real time and promptly adjust treatments to hasten the resolution of nonhealing wounds. Histologic and biochemical characterization of biopsied wound tissue, which is currently the only reliable method for wound assessment, is invasive, complex to interpret, and slow. Here we demonstrate the use of Raman microspectroscopy coupled with multivariate spectral analysis as a simple, noninvasive method to biochemically characterize healing wounds in mice and to accurately identify different phases of healing of wounds at different time-points. Raman spectra were collected from "splinted" full thickness dermal wounds in mice at 4 time-points (0, 1, 5, and 7 days) corresponding to different phases of wound healing, as verified by histopathology. Spectra were deconvolved using multivariate factor analysis (MFA) into 3 "factor score spectra" (that act as spectral signatures for different stages of healing) that were successfully correlated with spectra of prominent pure wound bed constituents (i.e., collagen, lipids, fibrin, fibronectin, etc.) using non-negative least squares (NNLS) fitting. We show that the factor loadings (weights) of spectra that belonged to wounds at different time-points provide a quantitative measure of wound healing progress in terms of key parameters such as inflammation and granulation. Wounds at similar stages of healing were characterized by clusters of loading values and slowly healing wounds among them were successfully identified as "outliers". Overall, our results demonstrate that Raman spectroscopy can be used as a noninvasive technique to provide insight into the status of normally healing and slow-to-heal wounds and that it may find use as a complementary tool for real-time, *in situ* biochemical characterization in wound healing studies and clinical diagnosis.

Nearly 6.5 million people in the United States suffer from chronic wounds leading to annual treatment costs that exceed $25 billion.[1] A wide variety of treatment options exist,[2] but finding a specific treatment that is effective for each wound is challenging. Clinicians often try multiple treatments until one is found that promotes the healing process for a particular patient. Analytical technologies and methods that would allow the clinician to accurately and quickly assess the status of a wound to

Received: October 22, 2013
Accepted: February 21, 2014
Published: February 21, 2014

   dx.doi.org/10.1021/ac500513t | *Anal. Chem.* 2014, 86, 3764−3772

assist in targeting therapy would be a significant contribution to clinical wound management.

In concept, wound healing is thought to occur in distinct, overlapping stages; it begins with hemostasis, is followed by a stage in which inflammation is prevalent, which in turn leads to a stage where formation of granulation tissue, cell proliferation, angiogenesis and re-epithelialization are dominant.[3] Nonhealing or slowly healing (dysregulated or chronic) wounds are frequently characterized as being stuck in a persistent, inflammatory stage, unable to make a transition to the cell-proliferative stage. The evaluation of nonhealing wounds is difficult, however, and is usually performed qualitatively based on gross visual examination[4] that requires high clinical skill and experience.[5] It may also sometimes require biopsies at multiple locations of a wound with concomitant wait for histological analyses.[6] A simple and fast method that characterizes healing progress in a wound has the potential to expedite clinical assessment, better inform treatment, ultimately reducing discomfort and promoting favorable wound healing outcomes for patients.

Several noninvasive, optical methods have shown promise for characterization of the physical properties of wounds *in vivo* such as cutaneous blood flow with assessment of wound microcirculation (laser Doppler perfusion imaging), tissue structure (optical coherence tomography), and tissue temperature (thermal imaging).[7] Currently, however, biochemical characteristics of healing wound beds can reliably be evaluated only by tissue biopsy followed by histology or chemical analysis.[8] In addition to being invasive, this method is tedious, laborious,[9] and subjective.[10] Raman spectroscopy, in contrast, holds the potential to provide a simple and rapid method that permits assessment of the biochemistry of a wound bed *in situ* and thus an alternative to traditional approaches to the biochemical evaluation of wounds that are based on biopsied tissue or wound fluids.[11] Raman spectroscopy relies on the inelastic (Raman) scattering of photons incident on a material. While most of the incident light is scattered elastically (without change in wavenumber), a small fraction (10^{-4} to 10^{-3} of the incident light intensity) is scattered inelastically with altered wavenumbers and these alterations (known as Raman shifts) correspond to transitions between rotational or vibrational energy levels of chemical bonds.[12] The Raman scattered light can be used to identify the chemical functional groups of a material.[13] Various biological tissues have been analyzed by Raman spectroscopy and shown to identify diseased tissue in ailments such as breast cancer,[14] atherosclerosis,[15] cervical precancer,[16] and Alzheimer's disease,[17] to name a few. Prior studies[18−21] have reported Raman spectra of wounds but no study has demonstrated the use of the method to distinguish between different stages of wound healing *in vivo*. In particular, we comment that past analyses of Raman spectra of *in vivo* wounds have been based on differences in individual Raman peaks or peak ratios that were assigned to specific proteins.[18−20] This approach is limited in diagnostic utility with complex biological tissue because many different tissue components are derived from common molecular structural units (amino-acids, sugars, fatty acids) and bonds. In contrast, we demonstrate that Raman spectra can provide useful biochemical insights into wound healing when peak locations and intensities are considered in aggregate across the entire Raman spectrum. Multivariate statistics, as used in our study, enable the evaluation of aggregate differences in spectra across a wide wavenumber range resulting in a "spectral signature" characteristic of individual phases of the wound healing process. Our study employs Raman spectroscopy in a well-characterized animal wound model, the excisional "splinted" wound in the mouse that mimics the healing of full-thickness wounds in humans.[22] We demonstrate a methodology to distinguish between different stages of wound healing on the basis of an aggregate of biochemical markers (associated with the different stages) that are identified by Raman spectroscopy. Raman spectra that are collected from a wound are subjected to multivariate factor analysis (MFA) to yield analogous factor "loadings" which serve as objective, quantitative measures in the assessment of healing of the wounds.

In the remainder of this paper, we first discuss differences in averaged Raman spectra collected from wounds at different time-points by assigning peak locations and areas to chemical bonds that correspond to amino-acids or protein secondary structures. Second, we employ multivariate factor analysis (MFA)[23,24] to interpret the Raman spectra and distinguish between the different phases of wound healing in a quantitative and objective manner. This approach is complemented by histopathologic imaging of biopsied tissue. Third, we show that the abstract factors obtained from MFA can be correlated to major wound bed constituents that are associated with the different phases using non-negative least squares (NNLS) fitting of the factor score spectra with basis spectra. Fourth, we show that variability in healing between wounds in different mice can be quantified with the help of MFA and "outlier" (slow-to-heal) wounds can also be identified, and we further confirm our results using histopathologic analysis.

MATERIALS AND METHODS

Creation of Full Thickness Dermal Wounds in Mice and Harvesting of Wounds. All experimental protocols were approved by the Institutional Animal Care and Use Committee of the University of Wisconsin-Madison. BalbC mice (Jackson Laboratories, Inc., Bar Harbor, ME) between the ages of 8 to 16 weeks were used for the studies. Please refer to the Supporting Information for details on mice upkeep. Mice were anesthetized with 2% inhaled isoflurane, administered using an induction chamber. The mice were injected with buprenorphine (0.001 mg) for analgesia prior to wounding. Mice were shaved on the cranial dorsal region and back nails trimmed. Shaved area was aseptically prepped with Betasept Scrub (4% chlorhexidine gluconate) and sterile saline (0.9%) 3 times each using sterile cotton tipped applicators. Silicone splints (11 mm × 1.75 mm O-ring, O-Ring Warehouse no. 0568-013) were glued to the skin, one on each side of the midline with CrazyGlue Gel. Six simple interrupted sutures were placed with 5-0 nylon suture (Monosef, Covidien or Ethilon; Ethicon) with the suture equidistant around the O-ring. Two 6 mm wounds, one within each splinted skin area, were created using a 6 mm biopsy punch (Milltex, Inc., Plainsboro, NJ). For wounds not being harvested at the initial time point, a 14 mm plastic coverslip was glued to the splint with CrazyGlue Gel and then covered with Tegaderm (3M). Mice were recovered from anesthesia on a warming pad until ambulatory and then returned to the colony. Upon completion of each time point, the mice were euthanized with an intraperitoneal injection of Beuthanasia-D (Schering-Plough, Kenilworth, NJ) solution (0.5 mL per mouse) after induction of anesthesia as described above.

Wounds were harvested for collection of Raman spectra and histopathologic analysis using iris scissors and eye dressing forceps. A square of tissue was cut around the outside of the O-ring and placed in a tissue cassette for later placement in 10%

dx.doi.org/10.1021/ac500513t | Anal. Chem. 2014, 86, 3764−3772

formalin. Please refer to the Supporting Information for detailed methods for histopathologic analyses of the wounds.

Experiments were repeated on four separate batches of mice (designated as WT1 to WT4 in the manuscript) at different times following the same protocol as above. Histopathologic analysis was performed on all mice wounds belonging to batches WT3 and WT4. In batch WT2, histopathologic analysis was performed on half of the wounds and Raman spectra was collected from the other half of the wounds. Table 1 indicates the no. of mice in different batches assigned for harvesting of wounds at different time-points.

Table 1. Number of Mice in Different Batches According to Time-Point of Harvesting of Wounds

batch/no. of mice	day 0	day 1	day 5	day 7
WT1	4	4	4	
WT2	4	5	5	
WT3	6	7		7
WT4	3	5	5	5

Raman Spectral Analysis. A confocal Raman microscope (Thermo Fisher Raman DXR) with a 10× objective (N.A. 0.25) and a laser wavelength of 532 nm (10 mW of power at sampling point) was used to collect spectra. The estimated spot size on the sample was 2.1 μm and resolution was 2.7−4 cm^{-1}. The confocal aperture used was a 25 μm pinhole, and spectra between wavenumbers 500−3500 cm^{-1} were collected. A total of 5−6 spectra were collected from 6 different points across the surface of the wound bed (top left, top right, one or two from the center, bottom left, bottom right, see Figure S-1 in the Supporting Information). In general, spectra acquired from distinct spatial locations differed from each other, reflecting spatial heterogeneity on the wound bed surface (see Figure S-2 in the Supporting Information). As discussed below, we averaged these spectra in the study reported in this paper. The collection time for each spectrum was around 5 min. Spectra were also collected for 7 pure components: bovine collagen (Sigma-Aldrich, St. Louis, MO), bovine elastin (Sigma-Aldrich, St. Louis, MO), hyaluronic acid (Lifecore Biomedical, Chaska, MN), fibronectin (Biomedical Technologies, Stoughton, MA), fibrin (Sigma-Aldrich, St. Louis, MO), mouse blood drawn as per approved protocol (Institutional Animal Care and Use Committee, University of Wisconsin-Madison), and triolein (Sigma-Aldrich, St. Louis, MO) for comparison to the spectra obtained from the wound beds. Proprietary features available in OMNIC (Thermo Scientific) software were used to remove background fluorescence from all the spectra using polynomial baseline fitting (6th order) and to normalize the spectra. As mentioned above, spectra collected from different locations on a particular wound were averaged to represent an individual wound. The spectra representing individual wounds characterized on the same day were averaged again so that each day (day 0/1/5/7) was represented by one spectrum (see Figure 2). The standard deviation for these spectra has been presented in Figure S-3 (in the Supporting Information). An analysis of peak areas and peak locations was performed for these averaged spectra, and the spectral peaks were curve-fitted and analyzed for peak positions and peak areas using Fityk.[25]

Multivariate factor analysis was performed on all spectra representing individual wounds using XLSTAT version 2013.1.02 (MS Excel add-in) to express the spectra as a weighted sum of 3 "factor score spectra" with the weights termed as "factor loadings". Please refer to the Supporting Information (Multivariate Factor Analysis section) for more details.

Factor scores were also normalized and scaled to convert them into "factor score spectra" which were fitted with real spectra belonging to the 7 different wound bed constituents using Non-Negative Least Squares (NNLS) analysis using MATLAB (v. R2012b) to correlate the factor score spectra with spectra of the 7 pure wound bed constituents. The degree of orthogonality between the spectra of pure wound bed constituents was also calculated to establish the differences between them (refer to the Supporting Information for details). The degree of orthogonality was calculated between different pairs of the basis spectra using MATLAB and it was determined to range between 0.38 and 0.94 (see Table S-1 in the Supporting Information). For the NNLS analysis, R^2 (coefficient of multiple correlation) > 0.9 for all factor score spectra. A Ryan-Einot-Gabriel-Welsch Q multiple comparison test (REGWQ test, ANOVA) for determining the significance of differences (confidence interval, 95%) between sets of factor loading values for wounds on different days was also performed and the results are presented in Table S-2 (in the Supporting Information).

RESULTS

Analysis of Averaged Raman Spectra of Mice Wounds on Days 0, 1, 5 and 7. On the basis of prior histopathologic analysis of full thickness murine wounds in our laboratory, we chose 4 time-points (0, 1, 5, and 7 days) at which to collect Raman spectra from wounds to characterize biochemical changes that occur as wounds progress through different stages of healing (hemostasis, inflammation, granulation/proliferation). Figure 1 shows representative images of splinted wound beds obtained at the different time-points. The appearance of the wound bed surface in all the wounds varied little at different time-points, except for a slight increase in size from day 0 to day 1 and then a marked reduction in wound size by the seventh day. Histopathologic scores for inflammation and granulation were consistent with the wounds at different times corresponding to different stages of healing (see below and refer to the Supporting Information for Figures S-4 to S-7 and Table S-3).

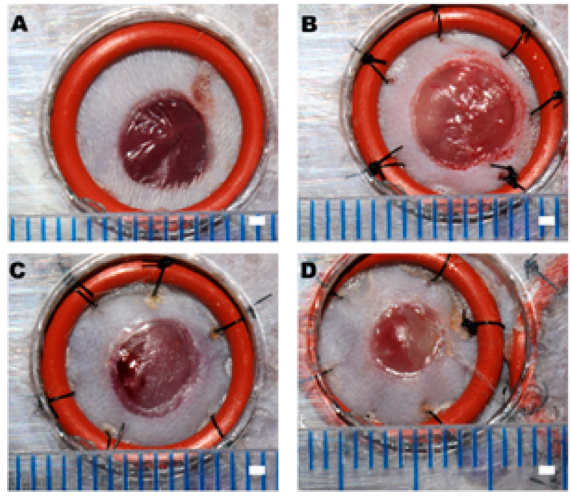

Figure 1. 'Splinted' wounds in mice on (A) day 0, (B) day 1, (C) day 5, and (D) day 7. Scale bar = 1 mm.

Figure 2 shows the Raman spectra of the wounds at the different time points (refer to Table S-4 in the Supporting Information for a detailed summary of peak locations and areas).

dx.doi.org/10.1021/ac500513t | Anal. Chem. 2014, 86, 3764−3772

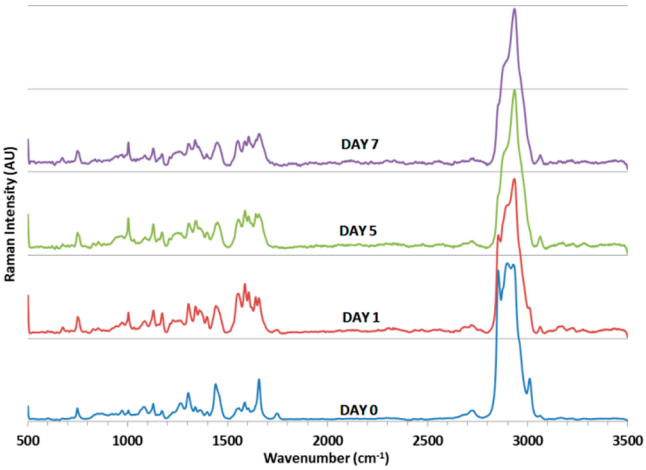

Figure 2. Averaged Raman spectra of mice wounds on day 0 (n = 30), day 1 (n = 36), day 5 (n = 23), and day 7 (n = 23).

The prominent Raman peaks in the spectra can be grouped into three categories: (i) peaks related to the strong amide I (WN, 1620−1680 cm^{-1}) and amide III (WN, 1220−1270 cm^{-1}) vibrational modes for the peptide backbone, which indicate different protein secondary structures,[26] (ii) peaks that correspond to specific side-chains for specific amino-acids (WN, 674, 749, 785, 826, 851, 1003, 1030, 1172, 1338, 1360, 1398, 1585, 1606 cm^{-1}) making up the proteins,[27] and (iii) peaks corresponding to the −CH stretching region at higher wavenumbers (WN, 2700−3100 cm^{-1}) which indicate relative quantities of total protein and lipid.[28] From these groupings, we make three observations. First, the decrease in areas of multiple peaks corresponding to α-helical secondary structure (WN, 1267, 1655 cm^{-1}) and a simultaneous increase in areas for peaks representing β-sheets (WN, 1223, 1623, 1638 cm^{-1}) and random coils (WN, 1244, 1671 cm^{-1}) across the Amide I and Amide III vibrational regions indicate the deposition of new proteins on a wound bed which initially contained residual ECM collagen (α-helical). Fibrin, collagen type III, fibronectin, elastin, hyaluronic acid, and cells and proteins in blood plasma are generally the major constituents of granulation tissue that forms on the wound bed in the course of healing. Fibrin is a key protein forming the blood clot and granulation tissue and has high nonhelical (β-sheet + random coil ∼80%) secondary structure content.[29] Fibronectin is another key protein that forms the provisional matrix on a wound during the first week of wound repair,[30] and it also has a high content (∼80%) of β-sheets (WN, 1637, 1679, 1225 cm^{-1}) in particular.[31] Second, most peaks which correspond to amino acids (WN, 674, 749, 785, 1003, 1360 cm^{-1}) are observed to have a 2−4-fold increase in area, and this is again consistent with protein accumulation on the wound bed. Third, peak areas that are lipid specific (WN, 2852, 2933, 3010 cm^{-1}) are reduced 1−4-fold with time and those that are protein-specific (WN, 2897, 2968, 3062 cm^{-1}) are increased 1−3-fold. This result is consistent with subcutaneous fat (that is exposed when a full-thickness wound is created) being overlaid with granulation tissue. We note, however, that many peak locations suffer from redundancy of assignment (as seen in Table S-4 in the Supporting Information) and individual peaks cannot be assigned with certainty to specific ECM proteins on the wound bed. Consequently, as detailed below, we sought to employ multivariate statistical methods to distinguish between wound spectra based on aggregate differences measured across a wide wavenumber range.

Multivariate Factor Analysis (MFA) of the Spectral Data Set and Non-Negative Least-Squares (NNLS) Fitting of Factor Score Spectra. As described in the Materials and Methods section, we used multivariate factor analysis (MFA)[23,24] to analyze the spectral data. Our goal was to test the hypothesis that changes in composition of a wound that accompany changes in the stage of healing give rise to Raman spectra that can be deciphered using MFA to yield unique spectral signatures that form underlying basis Raman spectra for each stage of healing. Eigenanalysis of the correlation matrix formed from the spectral data matrix revealed that there were three eigenvectors whose eigenvalues were greater than 1 (see Figure S-8 (scree plot) in the Supporting Information) and that 99% of the variability in the spectral data set could be expressed in terms of them. However, the factors calculated initially from the eigenvector matrix were orthogonal and therefore uncorrelated. Our next goal was to identify factors which would not necessarily be uncorrelated but could model the levels of biochemical constituents associated with the different stages of healing (which are correlated) and would resemble non-negative, real spectra. We therefore relaxed the orthogonality constraint and performed oblique rotations of the factor axes (Promax rotation[32]) which increases the simplicity of interpretation,[33] makes each variable (wound spectrum) identify with one or a small proportion of the factors (and thus enable clustering of similar variables on basis of their factor loadings),[24] spreads the variance across factors more evenly,[24] and generates an invariant factor solution[24] (that does not depend on the particular mix of variables involved and is generalizable across experiments). We found that the resulting factor score "spectra" were able to resemble non-negative, "real" spectra (see Figure S-9 in the Supporting Information) and we hypothesized that these could be assigned as spectral signatures for the different stages of healing. We verified this prediction by obtaining a high degree of fit between each factor score spectrum and spectra obtained from pure wound bed constituents using non-negative least-squares fitting (results described further below).

Figure 3A shows the factor scores (scaled and normalized) obtained from MFA plotted against wavenumber. Figure 3B shows averaged factor loading values for all wounds harvested at a particular time-point. A distinct pattern of factor loading values can be observed for each time-point (values sum to 1 at each time-point) which in turn corresponds to different stages of wound healing. While factor 1 loading is seen to decrease with time, factor 2 and factor 3 loadings conversely increase with time. We speculated that factor 1 is likely correlated with the fresh state of a wound whereas factors 2 and 3 probably represent the accumulation of cells and proteins that are associated with inflammatory stage and deposition of granulation tissue, respectively. Consistent with our hypothesis, Figure 3B shows that the average loading value for factor 1 is reduced by 50% (from 0.84 ± 0.03 to 0.41 ± 0.05) and factor 2 is increased 6−7-fold (from 0.07 ± 0.02 to 0.48 ± 0.05) between day 0 and day 1. On day 5, the factor 1 loading value is reduced even further to 15% of its initial value (from 0.84 ± 0.03 to 0.13 ± 0.03), factor 2 remains the same, and factor 3 loading increases 4-fold (from 0.1 ± 0.02 to 0.42 ± 0.06). The day 7 factor loadings were not found to be significantly different from day 5 (for details, refer to Table S-2 (Supporting Information)) except for a decrease in factor 2 loadings (to 0.27 ± 0.05).

On the basis of the above observations, we sought to determine if it was possible to associate each factor score spectrum to real wound bed constituents that are typically present during the course of healing. Our model consisted of

dx.doi.org/10.1021/ac500513t | Anal. Chem. 2014, 86, 3764−3772

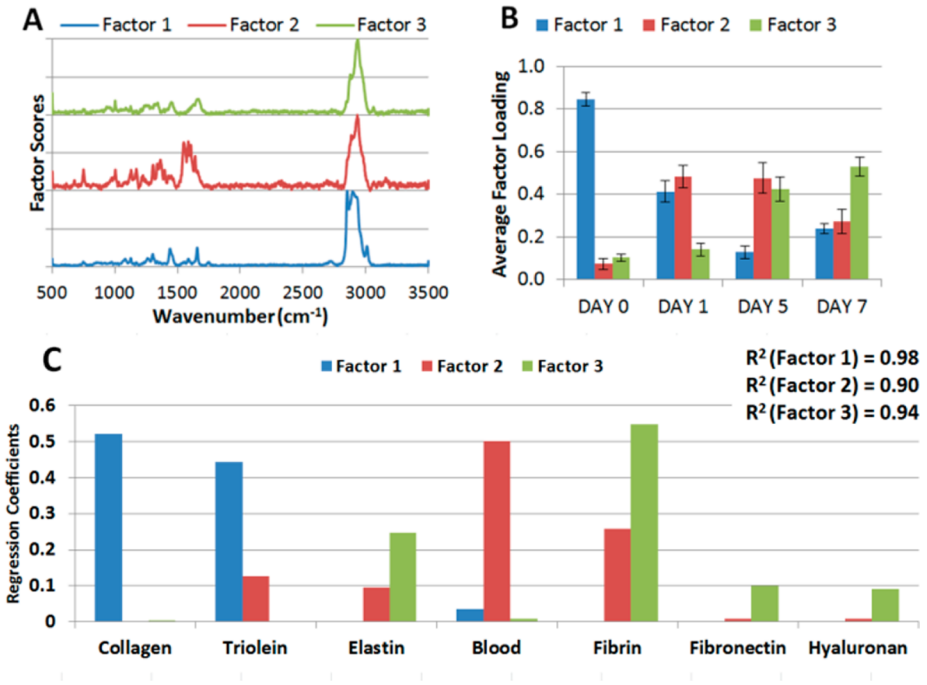

Figure 3. (A) Factor score spectra (normalized and scaled) from MFA and (B) average factor loadings from MFA (normalized and scaled). Error bars indicate ±SEM. (C) Standardized regression coefficients of model basis spectra of wound bed constituents for the factor score spectra.

basis spectra from 7 major wound bed constituents (see Figure S-10 for basis spectra and Table S-5 for their Raman bands in the Supporting Information), and the factor score spectra could be depicted as an aggregate of these basis spectra with a high degree of fit (R^2 values > 0.90) using Non-Negative Least Squares (NNLS) analysis. Figure 3C shows the standardized regression coefficients (RC) for the basis spectra which collectively sum to 1 for each factor score spectrum. Figure 3C indicates that Factor 1 score spectrum has strong contributions from collagen (RC, 0.52) and triolein (RC, 0.44; a triglyceride that mimics subcutaneous fat[34]), components that correlate strongly to the fresh state of a full-thickness wound bed. Factor 2 score spectrum has high contributions from blood (RC, 0.50, which contains inflammatory cells) and fibrin (RC, 0.26), components that represent inflammation on the wound bed as healing progresses[35] and minor contributions from triolein (RC, 0.12), elastin (RC, 0.1), hyaluronic acid (RC, 0.01), and fibronectin (RC, 0.01). Factor 3 score spectrum has strong contributions from fibrin (RC, 0.54), elastin (RC, 0.24), hyaluronic acid (RC, 0.1), and fibronectin (RC, 0.1) all of which are key components of granulation tissue on the wound bed and reflect a high proclivity of the wound toward cell proliferation which would lead to wound closure.[35]

Distinction between Individual Wounds on the Basis of Factor Loading Values. MFA enables a simple way to quantify the variability among the different spectra by comparing factor loading values. Here we show that this can be used to distinguish between individual wounds in different healing stages. Figure 4 shows the clustering of wounds (from the experiment on the batch of mice "WT3") which belong to similar stages of healing based on their factor loadings. They are plotted graphically in a 3D graph where the axes represent two of the factors, and the size of circles belonging to different wounds represents the third factor. While all wounds harvested on day 0 were similar to each other in their spectra and hence had loading values close to each other, 4 wounds from later time-points (day 1 and day 7) behaved as "outliers" whose loading values corresponded to earlier time points (day 0 or day 1 respectively) and are highlighted with solid red labels in Figure 4. Specifically, the outlier wound for the set of wounds harvested on day 7 (WT3 Day 7 S13) has low factor 1 and factor 3 loading values (0.132 and 0.355, respectively) but a high factor 2 loading value (0.554). We compared this observation with histopathologic imaging of the wound sections (see Figure 5E,F) which also shows the "outlier" wound to be exhibit reduced healing in terms of granulation scores and re-epithelialization (which we have associated earlier with factor 3 on basis of NNLS fitting) but has high inflammation (associated with factor 2). Again, three wounds were evaluated as outliers among those harvested on Day 1 (WT3 Day 1 S6, S9, and S10) with high factor 1 loading values and low factor 2 and 3 loading values. This is consistent with histopathologic images of sections from 2 out of the 3 wounds (WT3 Day 1 S6 and S9; see Figure 5A–D) which indicate an inflammation score that is lower than typical day 1 wounds and an overall appearance similar to day 0 wounds. The clustering of wounds on the basis of their healing states was broadly consistent across the multiple groups used in repeat experiments (see Figure S-11 in the Supporting Information).

DISCUSSION

When a full-thickness dermal wound is initially created in mice, subcutaneous fat and residual ECM collagen is exposed and composes the starting wound bed surface. Significant biochemical changes occur on the wound bed within the first day of wounding, when hemostasis is established and an inflammatory response is mounted.[36] As a result, a provisional matrix principally made up of fibrin and fibronectin is deposited on the wound bed that is infiltrated with inflammatory cells (neutrophils, macrophages) and burst platelets from blood. While this wound bed activity is not apparent by gross physical appearance of the wounds alone (see Figure 1A,B), it is evidenced in the notable differences in factor loading values

dx.doi.org/10.1021/ac500513t | Anal. Chem. 2014, 86, 3764−3772

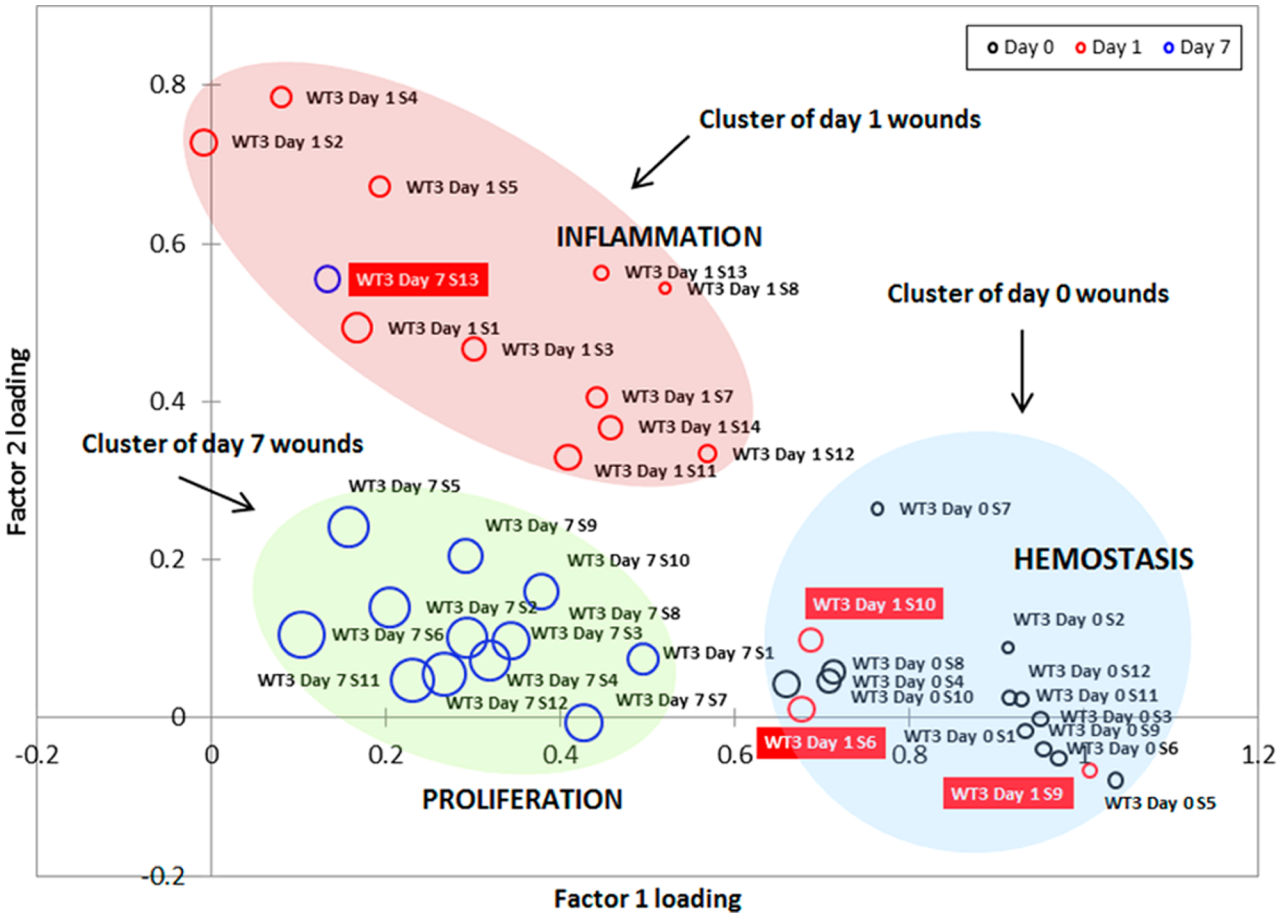

Figure 4. Wounds cluster around three sets of factor loadings (based on Raman spectroscopic characterization) which represent different stages of healing. The axes represent factors 1 and 2 while the third factor is represented by the size of the circles. The wounds represented in this graph were from a single experiment (WT3) involving 12−14 wounds (S1−S14; created in 6−7 mice) that were characterized at each time-point (Day 0/Day 1/Day 7). Outliers indicate slowly healing wounds and are marked with red boxed labels. All the wounds were analyzed using histopathology.

obtained from Raman spectra between day 0 and day 1 (see Figure 3B), a decrease in factor 1 (associated with subcutaneous fat and residual ECM collagen) by 50% and an increase in factor 2 (associated principally with fibrin and blood) by 6−7-fold. The provisional matrix so formed is subsequently infiltrated by fibroblasts and remodeled into granulation tissue (which contains wound bed constituents such as hyaluronic acid, fibronectin, elastin, and collagen type III) while inflammation subsides. This activity is manifested in the changes to factor loading values as well, factor 2 decreases by day 7, factor 3 (associated principally with fibrin, fibronectin, hyaluronan, and elastin) increases progressively, and there is an increase in factor 1 (associated with collagen) also by day 7. Thus the 3 factors used to describe the spectra in our study successfully permit identification of the phase of healing for a particular wound on the basis of changes in quantities of underlying biochemical components. However, we note that NNLS fitting of factor score spectra with basis spectra can be improved further and higher R^2-values could potentially be achieved by increasing the number of basis components in our model. This issue will be addressed in future studies. We also note that in past studies,[18,20,37] analyses of Raman spectra of tissue have often relied upon band area ratios or band areas in the fingerprint (600−1800 cm^{-1}) and CH-stretching (2800−3100 cm^{-1}) region. However, such analyses did not prove sufficient for us to be able to uniquely identify the stages of healing in different wounds (see Table S-6 in the Supporting Information). For example, the band ratio 1665 cm^{-1}/1445 cm^{-1} which has been reported[20] to be indicative of collagen/total protein content does not permit identification of the stage of healing of the wound on different days; its values on day 1 (0.62) and day 7 (0.62) are the same. However, factor analysis is able to capture the differences between the spectra of those days as reflected in the average factor loadings (see Figure 3B).

The results presented in Figure 4 also indicate that wounds in individual mice with different extents of progress in their healing form distinct clusters on the basis of their factor loading values. The cluster analysis also identified "outlier" wounds which we hypothesized to indicate impairment in their healing, as murine wound healing progress is known to vary across individual mice.[38] Three out of four outlier wounds so identified could be associated with altered histopathologic profiles (see Figure 5). We note that histopathologic analysis suffers from a limitation of not always being representative of the entire wound, as it is based on microscopic examination of one section of the wound (passing through the central region of a wound). In our approach, spectra were collected from 5 to 6 different locations (size ~10 μm^2) distributed across each wound and were averaged to represent the entire wound (size ~20 mm^2). Our approach was designed for rapid collection of spectra from each wound bed surface (due to the large number of total wounds investigated). It is noteworthy that the factor loading values could still indicate the progress in healing of the wounds very well (see Figure 3B). However, the spatial heterogeneity of a wound is also an

dx.doi.org/10.1021/ac500513t | Anal. Chem. 2014, 86, 3764−3772

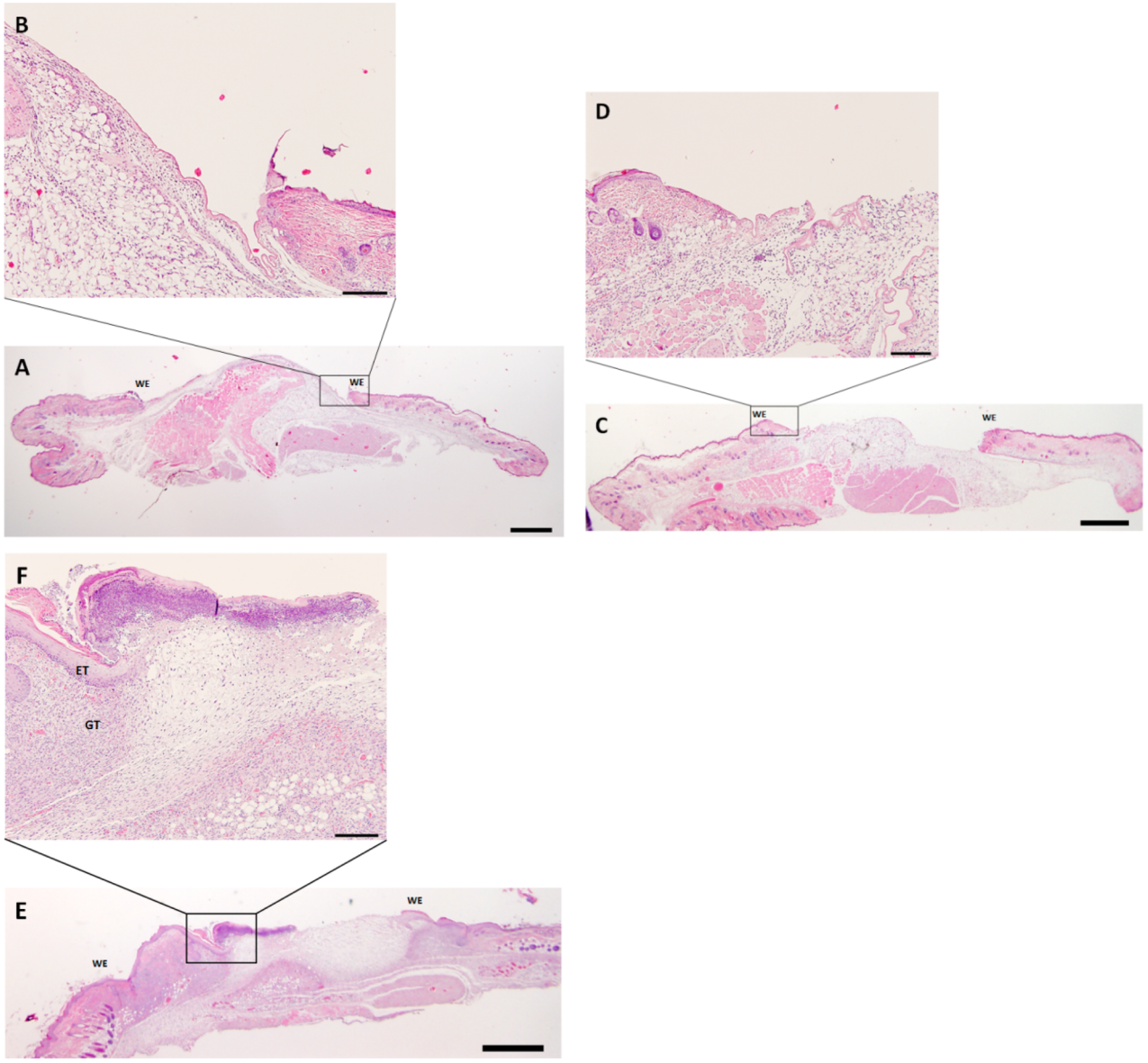

Figure 5. Hematoxylin and Eosin (H&E) stained sections of wounds. Hematoxylin is used to stain nuclei blue, while eosin stains cytoplasm and the extracellular connective tissue matrix pink. (A) H&E stained section of wound (WT3 Day 1 S6) indicated as an outlier by Raman spectral analysis in Figure 4. The appearance of the wound is similar to a day 0 wound (refer Figure S-4 in Supporting Information). Scale bar: 1 mm. (B) Magnified portion of the wound section (scale bar, 200 μm) shows a relatively lower level of inflammatory cells (blue dots) than a typical day 1 wound (refer Figure S-5 in Supporting Information). (C) H&E stained section of wound (WT3 Day 1 S9) indicated as an outlier by Raman spectral analysis in Figure 4. The appearance of the wound is similar to a day 0 wound. Scale bar: 1 mm. (D) Magnified portion of the wound section (scale bar, 200 μm) shows a relatively lower level of inflammatory cells (blue dots) than a typical day 1 wound (refer Figure S-5 in Supporting Information). (E) H&E stained section of wound (WT3 Day 7 S13) indicated as an outlier by Raman spectral analysis in Figure 4. The appearance of the wound indicates delayed healing relative to a typical day 7 wound. Scale bar: 1 mm. (F) Magnified portion of the wound section (scale bar, 200 μm) shows a higher level of inflammatory cells (blue dots), but a relatively lower level of granulation tissue formation than a typical day 7 wound (refer Figure S-7 in Supporting Information). WE = wound edge, GT = granulation tissue, ET = newly formed epithelial tissue.

important aspect of healing, and a Raman imaging approach could be used to create a map of biochemical features across a wound and to evaluate spatial differences in healing. This approach may lead to practical advantages in the clinic by informing selective therapeutic interventions such as discrete partial wound debridement that selectively targets areas of impaired healing while not disturbing areas of a wound that are progressing satisfactorily. Here we note also that it may be advantageous in future experiments to use a fiber optic sampler to enable (i) acquisition of Raman spectra directly from wounds in live animals and (ii) sampling of a larger fraction of the wound area. Finally, we comment that the predictive value of histopathologic assessments of inflammation and granulation tissue formation is diminished due to the inherent subjective and qualitative nature of the assessment technique.[10] In contrast, our approach provides an objective and semiquantitative measure of the healing progress in terms of factor loading values which are predictive of the healing status of the wound bed.

■ CONCLUSION

In summary, we have shown that the progress and stage of healing of wounds can be accurately evaluated in terms of

dx.doi.org/10.1021/ac500513t | *Anal. Chem.* 2014, 86, 3764−3772

biochemical changes occurring on the wound bed in a simple, noninvasive manner that combines Raman spectroscopy and spectral analysis. Specifically, we quantitatively tracked wound healing progress in terms of changes in key biochemical constituent that underlie the different stages of wound healing (e.g., inflammation and granulation) with the help of MFA/NNLS of Raman spectra obtained from murine full thickness dermal wounds. Furthermore, we demonstrated that we could distinguish between individual wounds at different stages of healing, including normally healing and slow-to-heal wounds. The results presented in this paper enable future studies of the biochemistry of a broad range of wound bed models (animal models, chronic wounds, wounds with biofilms). The results also offer substantial potential for translation to clinical practice, where wounds would be evaluated noninvasively by hand-held Raman spectrometers in conjunction with spectral analysis.

■ ASSOCIATED CONTENT

Supporting Information

Additional figures (11) , additional tables (6), and detailed methods as noted in the text. This material is available free of charge via the Internet at http://pubs.acs.org.

■ AUTHOR INFORMATION

Corresponding Authors

*E-mail: mcanultj@svm.vetmed.wisc.edu. Phone: +1 608 265 2455.
*E-mail: abbott@engr.wisc.edu. Phone: +1 608 265 5278.

Author Contributions

R.J. designed the experiments, performed the experiments, analyzed and interpreted the data, and wrote the paper. D.C. and P.R.K. performed the experiments. M.J.S., C.J.C. and C.J.M. interpreted the data. J.F.M. and N.L.A. designed the experiments, interpreted the data and wrote the paper.

Notes

The authors declare the following competing financial interest(s): The authors have filed a patent application on the work reported in this manuscript.

■ ACKNOWLEDGMENTS

We acknowledge the contribution of Dr. Richard Dubielzig in allowing us generous use of his microscope and other resources for histologic analysis and helpful discussions, Dr. Cindy Mattan-Bell for helpful discussions and suggestions, and Dr. Leandro Texeira for assistance with histopathologic scoring. This work was supported by the NIH Grant 1RC2AR058971, ARO Grants W911NF-10-1-0181 and W911NF-11-1-0251, and NSF through the Wisconsin MRSEC (Grant DMR-1121288).

■ REFERENCES

(1) Sen, C. K.; Gordillo, G. M.; Roy, S.; Kirsner, R.; Lambert, L.; Hunt, T. K.; Gottrup, F.; Gurtner, G. C.; Longaker, M. T. *Wound Repair Regener.* **2009**, *17*, 763−771.

(2) Sussman, C.; Bates-Jensen, B. M. *Wound Care: A Collaborative Practice Manual for Physical Therapists and Nurses*; Aspen Publishers: Gaithersburg, MD, 1998.

(3) Singer, A. J.; Clark, R. A. F. *New Engl. J. Med.* **1999**, *341*, 738−746.

(4) Hansen, G. L.; Sparrow, E. M.; Kokate, J. Y.; Leland, K. J.; Iaizzo, P. A. *IEEE Trans. Med. Imaging,* **1997**, *16*, 78−86. Mostow, E. N. *Clin. Dermatol.* **1994**, *12*, 3−9.

(5) Goldman, R. J.; Salcido, R. *Adv. Skin Wound Care* **2002**, *15*, 236−243.

(6) Bill, T. J.; Ratliff, C. R.; Donovan, A. M.; Knox, L. K.; Morgan, R. F.; Rodeheaver, G. T. *Ostomy/Wound Manage.* **2001**, *47*, 34. Alavi, A.; Niakosari, F.; Sibbald, R. G. *Adv. Skin Wound Care* **2010**, *23*, 132−139.

(7) Neidrauer, M.; Papazoglou, E. S. *Bioeng. Res. Chronic Wounds: A Multidiscip. Study Approach* **2009**, *1*, 381−404.

(8) Miteva, M.; Romanelli, P. *Meas. Wound Healing* **2012**, 155−173.

(9) Mark, M.; Teletin, M.; Antal, C.; Wendling, O.; Auwerx, J.; Heikkinen, S.; Khetchoumian, K.; Argmann, C. A.; Dgheem, M. *Curr. Protoc. Mol. Biol.* **2007**, 29B. 4.1−29B. 4.32.

(10) Morris, J. *Histopathology* **1994**, *25*, 123−128. Deolekar, M.; Morris, J. *Histopathology* **2003**, *42*, 227−232.

(11) Staiano-Coico, L.; Higgins, P.; Schwartz, S.; Zimm, A.; Goncalves, J. *Ostomy/Wound Manage.* **2000**, *46*, 85S.

(12) Keresztury, G. In *Handbook of Vibrational Spectroscopy*; J. Wiley: New York, 2002. Raman, C. V.; Krishnan, K. S. *Nature* **1928**, *121*, 501−502.

(13) Mulvaney, S. P.; Keating, C. D. *Anal. Chem.* **2000**, *72*, 145R−157R.

(14) Saha, A.; Barman, I.; Dingari, N. C.; Galindo, L. H.; Sattar, A.; Liu, W.; Plecha, D.; Klein, N.; Dasari, R. R.; Fitzmaurice, M. *Anal. Chem.* **2012**, *84*, 6715−6722. Mariani, M. M.; Maccoux, L. J.; Matthaus, C.; Diem, M.; Hengstler, J. G.; Deckert, V. *Anal. Chem.* **2010**, *82*, 4259−4263.

(15) Matthaus, C.; Dochow, S.; Bergner, G.; Lattermann, A.; Romeike, B. F. M.; Marple, E. T.; Krafft, C.; Dietzek, B.; Brehm, B. R.; Popp, J. *Anal. Chem.* **2012**, *84*, 7845−7851.

(16) Duraipandian, S.; Zheng, W.; Ng, J.; Low, J. J. H.; Ilancheran, A.; Huang, Z. W. *Anal. Chem.* **2012**, *84*, 5913−5919. Mo, J. H.; Zheng, W.; Low, J. J. H.; Ng, J.; Ilancheran, A.; Huang, Z. W. *Anal. Chem.* **2009**, *81*, 8908−8915.

(17) Hanlon, E. B.; Manoharan, R.; Koo, T. W.; Shafer, K. E.; Motz, J. T.; Fitzmaurice, M.; Kramer, J. R.; Itzkan, I.; Dasari, R. R.; Feld, M. S. *Phys. Med. Biol.* **2000**, *45*, R1−R59.

(18) Alimova, A.; Chakraverty, R.; Muthukattil, R.; Elder, S.; Katz, A.; Sriramoju, V.; Lipper, S.; Alfano, R. R. *J. Photochem. Photobiol. B: Biol.* **2009**, *96*, 178−183.

(19) Flach, C. R.; Zhang, G. J.; Mendelsohn, R. In *Emerging Raman Applications and Techniques in Biomedical and Pharmaceutical Fields*; Matousek, P., Morris, M. D., Eds.; Springer: New York, 2010; pp 365−384.

(20) Crane, N. J.; Brown, T. S.; Evans, K. N.; Hawksworth, J. S.; Hussey, S.; Tadaki, D. K.; Elster, E. A. *Wound Repair Regener.* **2010**, *18*, 409−416.

(21) Crane, N. J.; Elster, E. A. *J. Biomed. Opt.* **2012**, *17*, 0109021−0109028.

(22) Galiano, R. D.; Michaels, J.; Dobryansky, M.; Levine, J. P.; Gurtner, G. C. *Wound Repair Regener.* **2004**, *12*, 485−492.

(23) Lavine, B.; Workman, J. *Anal. Chem.* **2008**, *80*, 4519−4531.

(24) Rummel, R. J. *Applied Factor Analysis*; Northwestern University Press: Evanston, IL, 1970.

(25) Wojdyr, M. *J. Appl. Crystallogr.* **2010**, *43*, 1126−1128.

(26) Pelton, J. T.; McLean, L. R. *Anal. Biochem.* **2000**, *277*, 167−176. Dehring, K. A.; Smukler, A. R.; Roessler, B. J.; Morris, M. D. *Appl. Spectrosc.* **2006**, *60*, 366−372.

(27) De Gelder, J.; De Gussem, K.; Vandenabeele, P.; Moens, L. *J. Raman Spectrosc.* **2007**, *38*, 1133−1147.

(28) Tu, A. T. *Adv. Infrared Raman Spectrosc.* **1986**, *13*, 47−112. Gniadecka, M.; Nielsen, O. F.; Christensen, D. H.; Wulf, H. C. *J. Invest. Dermatol.* **1998**, *110*, 393−398. Gniadecka, M.; Nielsen, O. F.; Wessel, S.; Heidenheim, M.; Christensen, D. H.; Wulf, H. C. *J. Invest. Dermatol.* **1998**, *111*, 1129−1133.

(29) Tunc, S.; Maitz, M. F.; Steiner, G.; Vazquez, L.; Pham, M. T.; Salzer, R. *Colloids Surf., B: Biointerfaces* **2005**, *42*, 219−225. Schwinte, P.; Voegel, J. C.; Picart, C.; Haikel, Y.; Schaaf, P.; Szalontai, B. *J. Phys. Chem. B* **2001**, *105*, 11906−11916. Chen, Y. L.; Zhang, X. F.; Gong, Y. D.; Zhao, N. M.; Zeng, T. Y.; Song, X. Q. *J. Colloid Interface Sci.* **1999**, *214*, 38−45. Bramanti, E.; Benedetti, E.; Sagripanti, A.; Papineschi, F. *Biopolymers* **1997**, *41*, 545−553.

(30) Grinnell, F. *J. Cell. Biochem.* **1984**, *26*, 107−116. Clark, R. A. F.; Lanigan, J. M.; Dellapelle, P.; Manseau, E.; Dvorak, H. F.; Colvin, R. B. *J. Invest. Dermatol.* **1982**, *79*, 264−269.
(31) Osterlund, E.; Eronen, I.; Osterlund, K.; Vuento, M. *Biochemistry* **1985**, *24*, 2661−2667.
(32) Hendrickson, A. E.; White, P. O. *Br. J. Stat. Psychol.* **1964**, *17*, 65−70.
(33) Abdi, H. *Encyclopedia for Research Methods for the Social Sciences*; Sage: Thousand Oaks, CA, 2003; pp 792−795.
(34) Shafer-Peltier, K. E.; Haka, A. S.; Fitzmaurice, M.; Crowe, J.; Myles, J.; Dasari, R. R.; Feld, M. S. *J. Raman Spectrosc.* **2002**, *33*, 552−563.
(35) Baum, C. L.; Arpey, C. J. *Dermatol. Surgery* **2005**, *31*, 674−686.
(36) Midwood, K. S.; Williams, L. V.; Schwarzbauer, J. E. *Int. J. Biochem. Cell Biol.* **2004**, *36*, 1031−1037.
(37) Santos, L. F.; Wolthuis, R.; Koljenovic, S.; Almeida, R. M.; Puppels, G. J. *Anal. Chem.* **2005**, *77*, 6747−6752.
(38) Aberg, K. M.; Radek, K. A.; Choi, E. H.; Kim, D. K.; Demerjian, M.; Hupe, M.; Kerbleski, J.; Gallo, R. L.; Ganz, T.; Mauro, T.; Feingold, K. R.; Elias, P. M. *J. Clin. Invest.* **2007**, *117*, 3339−3349.